**Supplementary Information**

# The environmental liquid cell technique for improved electron microscopic imaging of soft matter in solution

Sana Azim*[1], Lindsey A. Bultema*[1], Michiel de Kock[1], Ernesto Rafael Osorio-Blanco[2], Marcelo Calderón[3,4], Josef Gonschior[1], Jan-Philipp Leimkohl[1], Friedjof Tellkamp[1], Robert Bücker[1], Eike C. Schulz[1], Sercan Keskin[5], Niels de Jonge[5,6], Günther Kassier[1], and R.J. Dwayne Miller[1,7]

[1]Max Planck Institute for the Structure and Dynamics of Matter, Luruper Chaussee 149, Geb. 99 (CFEL), 22761 Hamburg, Germany

[2]Freie Universität Berlin, Institute of Chemistry and Biochemistry, Takustr. 3, 14195 Berlin, Germany

[3] POLYMAT & Applied Chemistry Department, Faculty of Chemistry, University of the Basque Country UPV/EHU, Paseo Manuel de Lardizabal 3, 20018, Donostia-San Sebastián, Spain [4]IKERBASQUE, Basque Foundation for Science, 48013 Bilbao, Spain

[5]INM - Leibniz Institute for New Materials, Campus D2 2, 66123 Saarbrücken, Germany

[6]Department of Physics, Saarland University, Campus D2 2, 66123 Saarbrücken, Germany

[7]Departments of Chemistry and Physics, University of Toronto, 80 St. Georg Street, Toronto, Ontario M5S 3H6, Canada

* co-first authors, equal contribution

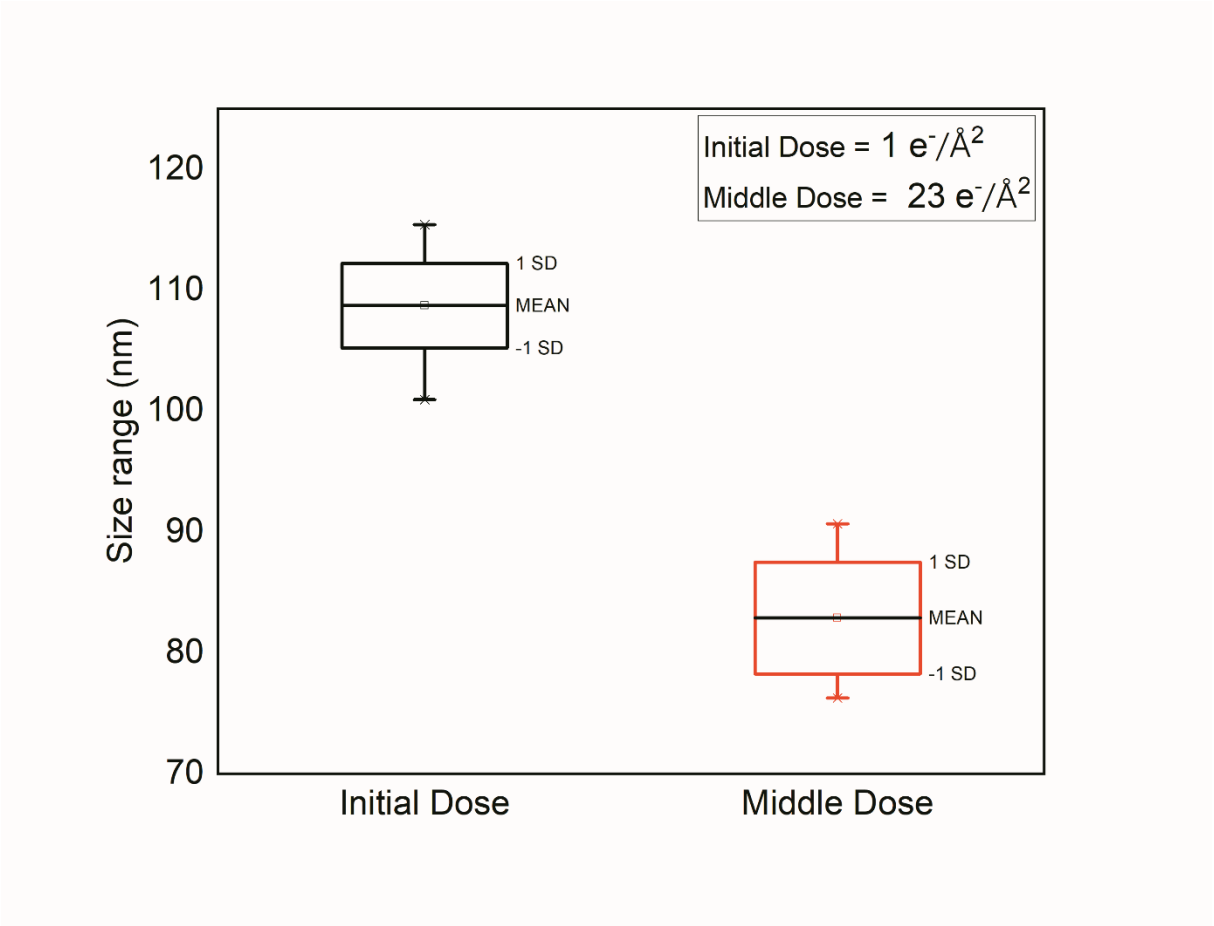


Figure S1: Box plot for PS particles.

*Shows the size range as determined using ImageJ and Origin, at initial dose of 1 $e^-/Å^2$ average particle size is 109 ± 3 nm, whereas after a cumulative dose of 23 $e^-/Å^2$ when the signal-to-noise ratio drops to its half value (middle dose) the size decreased to 82 ± 5 nm.*

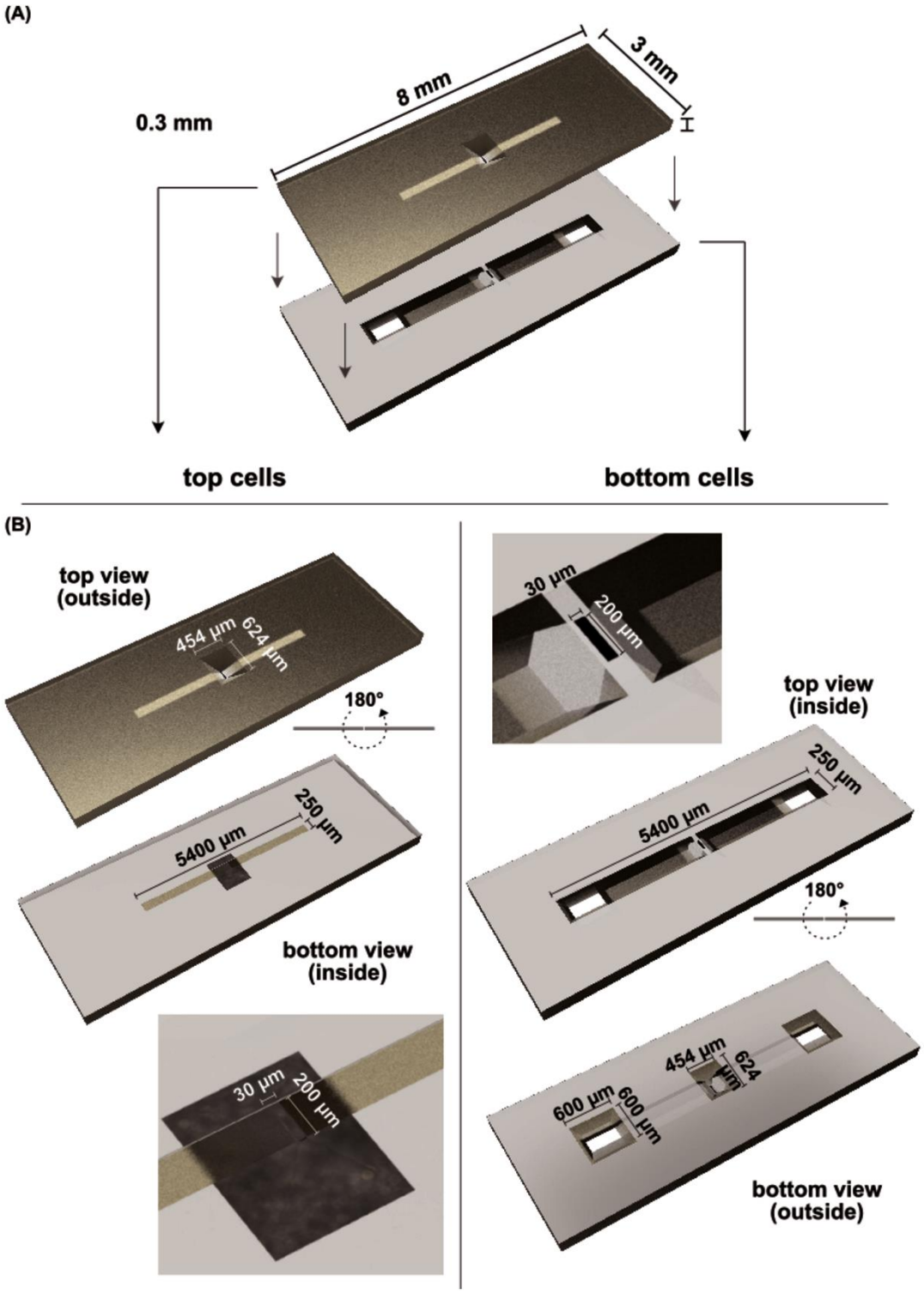


Figure S2. Liquid cell chip design and parameters.

*(A) Top and bottom parts of the liquid cell in the ELC (B) Magnified view top and bottom part of the liquid cell showing the silicon nitride window, flow channel, flow openings, and trenches.*

## Comparison of silicon nitride layer thickness as measured by the log ratio and parallax methods

To assess the accuracy of the log ratio method as given by equation 1, comparative parallax measurements were performed on selected silicon nitride films, where the lateral shift of features at various heights within the liquid cell is observed as a function of sample tilt angle (Liao, 2018). Due to the dimensions of our liquid cell holder, the degree of specimen rotation is limited to about 2°. Therefore, commercially available 3 mm format silicon nitride TEM grids of nominal thickness 20 nm and 50 nm (SimPore; SIN100-A20Q33 and Pelco; 21508-10) were examined in a Gatan 626 single tilt cryo transfer arm. The 20 nm silicon nitride films from SimPore are very similar to the films of our custom-made chips since they have the same nominal thickness and are from the same manufacturer (SimPore).

Gold nanoparticles of nominal diameter10 nm were deposited on both sides of the silicon nitride films, followed by mounting in the cryo transfer arm without filling the liquid nitrogen Dewar, and loading into the JEOL JEM 2100 TEM. The eucentric height was determined by rotating the specimen and adjusting the z- position until such rotation resulted in minimal specimen motion, followed by focusing the image through adjustment of the objective lens current. Regions on the silicon nitride films containing AuNP's on either side of the film were selected, and parallax measurements were performed by recording images corresponding to +20 +/- 0.1° and -20+/- 0.1° (40+/- 0.2° total rotation). Micrographs were recorded at a magnification of 20.000. ImageJ was used for further analysis. The parallax thickness $T$ was determined via Equation S1 (de Jonge et al., 2010; De Jonge et al., 2018):

$$T = \frac{\Delta L}{\sin \alpha} - 2r \qquad \text{S1}$$

where $\Delta L$ is the distance difference between a pair of particles (one on either side of the layer) corresponding to two images recorded at tilt angles of +α/2 and -α/2 (+20° and -20° in the present case). The distance between measured particle pairs is understood to be the distance

component in the image plane in the direction normal to the sample rotation axis. Assuming spherical particles of radius $r$ placed on the surface of the layer to be measured, the parallax thickness must be corrected by the term $2r$ as shown in Equation S1. Experimentally, $r$ was determined by the average diameter of five particles in each region. The four regions with a minimum of four particle pairs were averaged together.

**Table S1.** Average thickness as determined via parallax measurements.

| Nominal thickness from manufacturer (nm) | Parallax average thickness (nm) |
|---|---|
| 20 nm | 19.66 +/- 2.14 |
| 50 nm | 40.34 +/- 2.35 |

The transmission intensity ratio $I/I_0$ in Equation 1 in the main text is experimentally well approximated (in case of layer thicknesses less than the mean free path) by measuring the ratio of the total integrated intensity of images recorded with and without the objective lens aperture in place, respectively. This method is preferable to comparing intensities (with the objective aperture always in place) of images with and without a sample in the beam path respectively, since this would, in general, require the ability to temporarily withdraw the specimen from the beam path, or alternatively a highly stable beam the intensity of which could be calibrated before each measurement run. Neither of these requirements are met in our system, as typically measured beam intensity drifts are 8% per half hour. The pairs of images were recorded within a short period of time (less than 10 seconds) to minimize the effect of electron beam intensity drift. To account for the finite number of electrons scattered beyond the objective lens acceptance angle, which results in a small difference between the actual (no sample in the beam path) and measured (no objective aperture in the beam path) value of $I_0$, a comparison between

the transmission intensity at 10 different regions on silicon nitride covered and open regions (without an objective aperture inserted) were measured. Rapid translation from the silicon nitride covered regions to open areas (about 10 seconds) ensured negligible influence of beam intensity fluctuations. A ratio of 0.997 +/- 0.002 and 0.986 +/- 0.001 was measured in case of 20 nm and 50 nm nominal silicon nitride layers, respectively, and was used to correct the intensity ratio used for thickness calculations. It should be mentioned that the effect is small however, particularly in case of thin layers. The adjusted ratios were applied to the Reimer and molecular models, the Wentzel model approximates the potential with a single exponential function, while the molecular model uses the published scattering factors from Wang, which were calculated using configuration interaction wavefunctions (Reimer & Sommer, 1968; Kirkland, 2010; Wang et al., 1993; Reimer. L & Kohl. H, 2008). The following parameters were set for the thickness calculation: beam energy 200 keV; $Si_3N_4$ density =3200 kg/$m^3$; atomic weight= 0.02 kg/mol; effective atomic number= 10.6; objective aperture= 12.6 mrad. The results are shown in Table 2.

**Table S2.** The thickness determination based on the Reimer model and atomic models.

| Nominal thickness from manufacturer (nm) | Adjusted Ratio | Thickness from Reimer model (nm) | Thickness from atomic model (nm) |
|---|---|---|---|
| 20 nm | 0.920+/- 0.001 | 12.6 | 15.6 |
| 50 nm | 0.840+/- 0.001 | 26.4 | 32.6 |

The log ratio method deviates from the parallax thickness measurement by 36 % if the Reimer model is used, whereas it is 21% in case of the atomic model. Since the log ratio method employed here relies on a number of assumptions regarding material parameters and electron scattering models, a significant difference in the thus determined thickness to the actual

geometric thickness is to be expected. Such differences have also been found by other authors (Zhang, H., Egerton, R.F., and Malac, 2010)

## Electron dose calibration

Electron dose calibration of the TVIPS TemCam F216 camera was performed prior to the quantitative measurements reported in this paper. Routines and features of the supporting software EM Menu 4.0 were used. The procedure was as follows:

1) The JEOL JEM2100 features a current density readout from the main (radius 8 cm) phosphor viewing screen. Since this readout may not be precise, or may have drifted since initial factory calibration, a correction factor $f = I_{screen}/I_{true}$ was determined. In order to measure the true actual current $I_{true}$, the custom ELC holder (Figure 1) was loaded with a sandwich of two top part chips with removed silicon nitride window layers, such that a suitably positioned electron beam can pass through the assembly without being scattered. An electron beam was generated, passing entirely through the open window sample holder assembly and impinging on the large phosphor screen, but not entirely covering it to ensure that the total current is measured. The phosphor current density readout was recorded and converted to the corresponding current by multiplying with the screen area $A_s = \pi r_s^2$ with the screen radius $r_s$= 8 cm. The sample holder was then displaced such that the beam no longer passed through the silicon window frames, instead impinging on the liquid cell assembly, which acts like a faraday cup. Since our ELC holder features an electrically isolated head part with a wire connection, the corresponding current can be readily measured. This was done using a Keithley 2614B sourcemeter. This sequence of measurements was repeated for various currents in the range of 2.5 nA – 83 nA, yielding a correction factor $f = I_{screen}/I_{true}$ = 0.72 +/- 0.04. The linearity of the correlation between these currents was high, with an $R^2$ value of 0.997. This correction factor was considered in the camera electron dose calibration below.

2) Flatfield and darkfield correction images were recorded with pixel counts up to 30.000 following the standard procedure in EM Menu 4.0.

3) In order to convert electron dose values in the plane of the phosphor screen to corresponding values in the camera plane, the post-magnification was determined. To this end, a diffraction grating replica with 2160 lines/mm (Pelco No. 603) was imaged on the phosphor screen such that 28+/-0.5 grating lines spanned the 16 cm screen diameter, implying a grating spacing of 0.57 cm at the screen. A comparative image taken with the camera yielded a grating spacing of 571 pixels, corresponding to 0.89 cm real space in the camera plane (the physical pixel size of the detector is 15.6 µm). The post-magnification factor relating camera to phosphor screen is thus $M_{cs}$ = 1.56. The current densities in the camera and screen planes, $J_c$and $J_s$, respectively, are related by $J_s = M_{cs}^2 J_c$.

4) The beam size was then increased to a radius larger than the phosphor screen. The current density readout of the JEOL JEM2100 was recorded and corrected using the factor $f$ determined in 1). An image of the beam was recorded with the camera, and the average count per pixel was determined. The measured screen current density $J_s$ was then used to compute the current density at the camera $J_c$ according to the relation given in 3). Comparing the average pixel count with the thus determined electron dose in the camera plane yields an electron sensitivity factor of 29 counts/electron, which was used to compute the electron dose for all images. We estimate that our dose calibration is accurate within about +/-10%. The low current densities were measured using the camera, and not the phosphor screen. In order to do this, the camera was calibrated by exposing it with a known current density as determined from the phosphor screen, thus determining the counts per electron factor of the camera. Measurement of current densities lower than is possible with the phosphor screen are then essentially enabled through extrapolation, which is justified by the sufficient linearity and sensitivity of the camera (TVIPS TemCam F216).

DE JONGE, N., POIRIER-DEMERS, N., DEMERS, H., PECKYS, D. B. & DROUIN, D. (2010). Nanometer-resolution electron microscopy through micrometers-thick water layers. *Ultramicroscopy* **110**, 1114–1119.

DE JONGE, N., VERCH, A. & DEMERS, H. (2018). The Influence of Beam Broadening on the Spatial Resolution of Annular Dark Field Scanning Transmission Electron Microscopy. *Microscopy and Microanalysis* **24**, 8–15.

KIRKLAND, E. J. (2010). *Advanced Computing in Electron Microscopy Second Edition*. second. Springer Science+Business Media, LLC.

LIAO, Y. (2018). *Practical Electron Microscopy and Database*. www.globalsino.com/EM/.

REIMER. L & KOHL. H (2008). *Transmission Electron Microscopy*. Springer Science + Business Media, LLC www.springeronline.com/series/624.

REIMER, L. & SOMMER, K. H. (1968). Messungen und berechnungen zum elektronenmikroskopischen streukontrast für 17 bis 1200 kev-elektronen. *Zeitschrift fur Naturforschung - Section A Journal of Physical Sciences* **23**, 1569–1582.

WANG, J. H., SAGAR, R. P., SCHMIDER, H. & SMITH, V. H. (1993). X-Ray Elastic and Inelastic Scattering Factors for Neutral Atoms Z = 2-92. *Atomic Data and Nuclear Data Tables* , **53**, 233–269.

ZHANG, H., EGERTON, R.F., AND MALAC, M. (2010). Local Thickness Measurement in TEM. *Microscopy and microanalysis* **16**, 6–7.